Modeling tumor control probability for spatially inhomogeneous risk of failure based on clinical outcome data

Lühr, A.; Löck, S.; Jakobi, A.; Stützer, K.; Bandurska-Luque, A.; Vogelius, I. R.; Enghardt, W.; Baumann, M.; Krause, M.;

Originally published:

July 2017

Zeitschrift für Medizinische Physik 27(2017), 285-299

DOI: https://doi.org/10.1016/j.zemedi.2017.06.003

Perma-Link to Publication Repository of HZDR:

https://www.hzdr.de/publications/Publ-25851

Modeling tumor control probability for spatially inhomogeneous risk of failure based on clinical outcome data

Modellierung der Tumorkontrollwahrscheinlichkeit für räumlich inhomogenes Rezidivrisiko basierend auf klinischen Daten

Armin Lühr[a,b,c,d,*], Steffen Löck[b], Annika Jakobi[b], Kristin Stützer[b], Anna Bandurska-Luque[b,e], Ivan Richter Vogelius[f], Wolfgang Enghardt[a,b,c,d,e], Michael Baumann[a,b,c,d,e], Mechthild Krause[a,b,c,d,e]

[a] *German Cancer Consortium (DKTK), Partner Site Dresden, Dresden, Germany*
[b] *OncoRay – National Center for Radiation Research in Oncology, Faculty of Medicine and University Hospital Carl Gustav Carus, Technische Universität Dresden, Helmholtz-Zentrum Dresden – Rossendorf, Dresden, Germany*
[c] *German Cancer Research Center (DKFZ), Heidelberg, Germany*
[d] *Helmholtz-Zentrum Dresden-Rossendorf, Institute of Radiation Oncology, Dresden, Germany*
[e] *Department of Radiation Oncology, University Hospital Carl Gustav Carus, Technische Universität Dresden, Dresden, Germany*
[f] *Department of Oncology, Rigshospitalet, University of Copenhagen, Copenhagen, Denmark*

Abstract

Purpose: Objectives of this work are 1) to derive a general clinically relevant approach to model tumor control probability (TCP) for spatially variable risk of failure and 2) to demonstrate its applicability by estimating TCP for patients planned for photon and proton irradiation.
Methods: The approach divides the target volume into sub-volumes according to retrospectively observed spatial failure patterns. The product of all sub-volume TCP_i values reproduces the observed TCP for the total tumor. The derived formalism provides for each target sub-volume i the tumor control dose ($D_{50,i}$) and slope ($\gamma_{50,i}$) parameters at 50% TCP_i. For a simultaneous integrated boost (SIB) prescription for 45 advanced head and

*Corresponding author
Email address: armin.luehr@OncoRay.de (Armin Lühr)

neck cancer patients, TCP values for photon and proton irradiation were calculated and compared. The target volume was divided into gross tumor volume (GTV), surrounding clinical target volume (CTV), and elective CTV (CTVE). The risk of a local failure in each of these sub-volumes was taken from the literature.
Results: Convenient expressions for $D_{50,i}$ and $\gamma_{50,i}$ were provided for the Poisson and the logistic model. Comparable TCP estimates were obtained for photon and proton plans of the 45 patients using the sub-volume model, despite notably higher dose levels (on average +4.9%) in the low-risk CTVE for photon irradiation. In contrast, assuming a homogeneous dose response in the entire target volume resulted in TCP estimates contradicting clinical experience (the highest failure rate in the low-risk CTVE) and differing substantially between photon and proton irradiation.
Conclusions: The presented method is of practical value for three reasons: It a) is based on empirical clinical outcome data; b) can be applied to non-uniform dose prescriptions as well as different tumor entities and dose-response models; and c) is provided in a convenient compact form. The approach may be utilized to target spatial patterns of local failures observed in patient cohorts by prescribing different doses to different target regions. Its predictive power depends on the uncertainty of the employed established TCP parameters D_{50} and γ_{50} and to a smaller extent on that of the clinically observed pattern of failure risk.

Zusammenfassung

Ziel: Ziele dieser Arbeit sind 1) einen allgemeinen klinisch relevanten Anzastz zur Modellierung der Tumorkontrollwahrscheinlichkeit (TCP) für räumlich variables Rezidivrisiko herzuleiten und 2) dessen Anwendbarkeit zu demonstrieren durch Abschätzen der TCP für Patienten, die für Photonen- und Protonentherapie geplant wurden.
Material und Methoden: Der Ansatz teilt das Zielvolumen auf in Teilvolumina entsprechend retrospektiv beobachteter räumlicher Rezidivverteilungen. Das Produkt aller Teilvolumen TCP_i Werte reproduziert den beobachteten TCP für den Gesamttumor. Der hergeleitete Formalismus stellt für jedes Teilvolumen i den Tumorkontrolldosis- ($D_{50,i}$) und Anstiegparameter ($\gamma_{50,i}$) bei 50% TCP_i zur Verfügung. Für eine simultane integrierte Boost (SIB) Verschreibung wurden bei 45 fortgeschrittenen Kopf-Hals-Tumor-Patienten TCP Werte für Photonen- und Protonenbestrahlung berechnet und verglichen. Das Zielvolumen wurde jeweils in Grosstumorvolumen (GTV), umgebenes klinisches Zielvolumen (CTV) und elektives CTV (CTVE) eingeteilt. Das Risiko für Rezidive in jedem dieser Teilvolumina wurde der Literatur ent-

nommen.
Ergebnisse: Handliche mathematische Ausdrücke für $D_{50,i}$ und $\gamma_{50,i}$ wurden für das Poisson und das logistische TCP Modell hergeleitet. Vergleichbare TCP Werte wurden für Photonen- und Protonenpläne der 45 Patienten unter Benutzung des Teilvolumen-Modells abgeschätzt, trotz höherer Dosiswerte (durchschnittlich +4.9%) in dem niedrig-Risko CTVE für Photonenbestrahlung. Im Gegensatz dazu resultierte die Annahme einer homogenen Dosiswirkung im gesamten Zielvolumen in TCP Werten, welche der klinischen Erfahrung deutlich widersprechen (die höchste Rezidivrate im niedrigrisiko CTVE) und welche sich substanziell zwischen Photonen und Protonenbestrahlung unterscheiden.
Schlussfolgerung: Die präsentierte Methode ist aus dreierlei Gründen zweckdienlich: Sie a) basiert auf empirischen klinischen Outcome-Daten, b) kann sowohl bei inhomogenen Dosisverschreibungen als auch verschiedenen Tumorentitäten und Dosis-Wirkungs-Beziehungen angewendet werden und c) besitzt eine komfortable kompakte Form. Der Ansatz kann dafür eingesetzt werden, zuvor in Patientenkohorten beobachtete räumliche Muster von Lokalrezidiven gezielt mit einer Umverteilung der verschriebenen Dosis zu behandeln. Die Vorhersagekraft hängt maßgeblich von den Unsicherheiten der verwendeten etablierten TCP Parameter D_{50} und γ_{50} ab und zu einem kleineren Ausmaß vom klinisch beobachteten Muster des Rezidivrisikos.

Keywords:
radiotherapy, dose-response modeling, TCP, inhomogeneous dose, head and neck cancer, proton therapy

---

1. Introduction

In radiotherapy, clinical dose response data have been accumulated for about a century to relate radiation dose with tumor response [1, 2]. Increasingly, the ability to shape the dose distribution has made it possible to irradiate tumors with homogeneous and well-controlled doses. Together with data on clinical outcome, tumor control probability (TCP) models and parameters could be established for different tumor entities [2–10]. Among these, both, empirical and mechanistic TCP models are available. The latter are based on tumor-cell radiobiology, which can handle tumors of different volumes, non-uniform dose distributions, and heterogeneous radiosensitivities. However, a remaining challenge is to obtain realistic numbers that parametrize the biological inhomogeneity in such TCP models from clinical data.

With advancing imaging techniques it became possible to study the spa-

tial distribution, i.e., pattern of treatment failures within patient cohorts, in detail based on follow-up scans [11]. It turned out that local failures are commonly non-uniformly distributed in the target volume [12, 13]. In such a case one would observe, e.g., more failures in areas associated with the pre-treatment gross tumor volume than in the surrounding clinical target volume or a decreasing probability for recurrences with increasing distance to the center of the tumor volume. Regarding head and neck treatments, most failures were consistently found in-field [14–17]. The observed non-uniform distribution of treatment failures probably results from a spatial variation in e.g. the oxygenation level or clonogen cell density in the tumor [10]. Treatment strategies have been proposed that increase the dose in regions that are considered to be of high-risk for treatment failure and some that even decrease the dose in low-risk areas [18–21].

In general, the causes of failures and their spatial distribution are not known prior to treatment. Functional imaging is one approach to estimate the (spatial) variability of the radiosensitivity within a tumor [13, 22]. It requires, however, an understanding of the underlying biological mechanisms to prospectively identify high-risk regions in a tumor (e.g., hypoxia) for individual patients [23]. Alternatively, spatial patterns of local recurrences observed in large patient populations can be analyzed – as was recently done for head and neck cancer [11, 12] – to estimate the spatially inhomogeneous risk of failure. These risk patterns are representative for a patient cohort instead of an individual patient. Such a data-driven approach is clearly empirical. In principle, it does not require knowledge of the underlying cause for an inhomogeneous risk of failure in the tumor but instead a pattern of failure map for a patient population. For those tumor sites, for which reliable failure maps become available, the dose prescription could be adapted with the goal to reduce the expected overall failure risk of a population.

The purpose of this work is to provide a framework for TCP modeling that incorporates the spatially inhomogeneous risk of failure within target volumes. It is based exclusively on clinical, i.e., empirical outcome data. First, we derive a convenient and compact approach to estimate the quantitative impact of the spatially inhomogeneous failure pattern on TCP. Subsequently, we demonstrate how to apply our approach based on a given failure map by estimating TCP for 45 head and neck cancer patients included in a treatment planning study, which dosimetrically compares photon and proton irradiation – in both cases prescribed with a simultaneous integrated boost (SIB).

2. Materials and Methods

Two frequently employed TCP models are the Poisson and the logistic model [10]. They both show a sigmoidal dose response and can be parametrized by D_{50}, the dose that yields a TCP of 50%, and γ_{50}, the normalized steepness of the TCP curve at the dose D_{50}. These TCP parameters are available in the literature for several tumor entities and endpoints [2, 9, 10].

2.1. Local failure driven sub-volume TCP model

We derive a failure pattern-driven TCP model that considers the target volume to consist of N sub-volumes, each of which may exhibit a different dose response characteristic. As input, the approach uses first, standard TCP parameters D_{50} and γ_{50}, which reproduce the overall probability for a treatment failure in a population, and second, observed *spatial* patterns of such treatment failures in the target volume. The derived approach results in N separate TCP curves – one for each target sub-volume i – labeled as TCP_i. Each of the TCP_i is specified by the parameter pair $(D_{50,i},\ \gamma_{50,i})$, which is expressed in a compact analytical form. Evaluating TCP_i at the dose level D_i in sub-volume i yields the tumor control probability of that sub-volume. The product of all TCP_i values yields the total TCP. Figure 1 schematically summarizes how the approach estimates the TCP for a patient given a spatially inhomogeneous risk of failure as well as dose distribution.

The target volume may be divided into N sub-volumes such that for each target sub-volume i the relative proportion of failures,

$$f_i(D_\mathrm{h}) = \frac{n_i(D_\mathrm{h})}{n(D_\mathrm{h})}\,, \tag{1}$$

is known, e.g., from a clinical study with the prescribed homogeneous dose D_h. The n_i and n are the number of failures that were observed in sub-volume i and in the entire target volume, respectively, in the study cohort. Note, all N target sub-volumes are disjoint, i.e., they do not overlap with each other and the sum of all sub-volumes equals the total target volume. Accordingly, the f_i of all sub-volumes sum up to unity. We denote the total TCP for the entire target volume for the (homogenous) dose D_h – for which all f_i are known – by

$$tcp = \mathrm{TCP}(D_\mathrm{h}; D_{50}, \gamma_{50})\,. \tag{2}$$

For a uniform dose D_h in the entire target volume, we require the product of all sub-volume TCP_i to fulfill the following two conditions

$$tcp \;\; = \;\; \prod_{i=1}^{N} \mathrm{TCP}_i(D_\mathrm{h})\,, \tag{3}$$

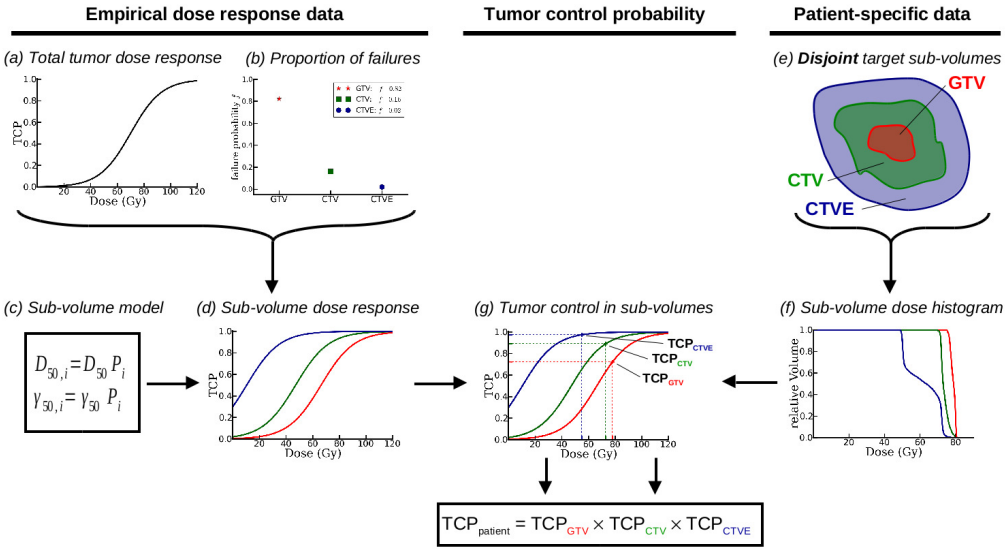

Figure 1: Schematic drawing of the target sub-volume tumor control probability (TCP) approach. Left column: Empirical data on (a) total TCP and (b) spatial failure pattern are used with the (c) derived model expressions to determine (d) a dose-response curve for each sub-volume. Right column: (e) disjoint target sub-volumes and (f) according dose distributions for a patient. Central column: for each sub-volume i a (g) TCP_i estimate (e.g., $\mathrm{TCP}_{\mathrm{GTV}}$) results from applying the corresponding (d) sub-volume TCP curve and (f) dose distribution. The product of all sub-volume TCP_i values yields the TCP of a patient.

$$\left.\frac{\mathrm{d}}{\mathrm{d}D}\mathrm{TCP}(D)\right|_{D_\mathrm{h}} \quad = \quad \left.\frac{\mathrm{d}}{\mathrm{d}D}\left(\prod_{i=1}^{N}\mathrm{TCP}_i(D)\right)\right|_{D_\mathrm{h}} , \tag{4}$$

i.e., the value and the slope of the product to be the same as for the total TCP at D_h.

Additionally, we introduce two assumptions that allow for deriving closed analytical expressions for the model parameters $\gamma_{50,i}$ and $D_{50,i}$. First, we use

$$\mathrm{TCP}_i(D_\mathrm{h}) \quad = \quad tcp^{f_i} , \tag{5}$$

to relate the proportion of failures f_i and the total TCP for a homogeneous target dose D_h with the sub-volume TCP_i. It automatically fulfills the condition in Eq. (3). Second, we assume the slopes at 50% TCP_i in all sub-volumes to be equal,

$$\frac{\gamma_{50,i}}{D_{50,i}} \quad = \quad \frac{\gamma_{50,j}}{D_{50,j}} = C \qquad \forall_{i,j} , \tag{6}$$

with C being a constant. In the following subsections 2.1.1 and 2.1.2, we provide convenient analytical expressions for $D_{50,i}$ and $\gamma_{50,i}$ for two common

TCP models, the Poisson and the logistic model. A detailed derivation can be found in the Appendix.

2.1.1. Poisson TCP model

The Poissonian form of the single hit TCP model for cell damage can be written as,

$$\mathrm{TCP}(D) = \exp\left[-\exp\left\{\ln(N_\mathrm{c}) - \alpha\, D\right\}\right] , \tag{7}$$

with N_c and α being the number of clonogen cells and the cell radiosensitivity, respectively. However, for clinical situations, the exact values for α and N_c are usually not available. Also, each patient has a distribution of tumor cells with different α values. For larger numbers of cells (Poissonian limit) of the same radiosensitivity these two parameters can be mathematically related to the parameters D_{50} and γ_{50} (as shown in [7] and references therein):

$$\ln(N_\mathrm{c}) = \frac{2}{\ln(2)}\,\gamma_{50} + \ln\left[\ln(2)\right] , \tag{8}$$

$$\alpha = \frac{2}{\ln(2)}\,\frac{\gamma_{50}}{D_{50}} . \tag{9}$$

Inserting Eqs. (8) and (9) into (7) yields the TCP expression,

$$\mathrm{TCP}(D) = \exp\left[\ln\left(\frac{1}{2}\right)\exp\left\{\frac{2\gamma_{50}}{\ln(2)}\left(1-\frac{D}{D_{50}}\right)\right\}\right] , \tag{10}$$

which is parametrized by the clinically accessible parameters γ_{50} and D_{50}. Note that these TCP expressions do not explicitly consider the response to different fraction sizes. Different fraction sizes could be handled by using fraction size corrected D values.

In order to fully describe

$$\mathrm{TCP}_i(D) = \exp\left[\ln\left(\frac{1}{2}\right)\exp\left\{\frac{2\gamma_{50,i}}{\ln(2)}\left(1-\frac{D}{D_{50,i}}\right)\right\}\right] . \tag{11}$$

in each of the N sub-volumes we have to determine all $2N$ sub-volume model parameters $\gamma_{50,i}$ and $D_{50,i}$. Using the conditions and assumptions in Eqs. (3)-(6) we arrive at the description of the sub-volume parameters,

$$D_{50,i} = D_{50}\, P_i , \tag{12}$$

$$\gamma_{50,i} = \gamma_{50}\, P_i , \tag{13}$$

with

$$P_i = 1 + \frac{\ln(2)}{2\gamma_{50}}\,\ln(f_i) , \tag{14}$$

as explicitly shown in Appendix A. Note that in the case of the Poisson model the ratio $\gamma_{50,i}/D_{50,i}$ is for each of the N sub-volumes equal to γ_{50}/D_{50} and therefore independent of the values of D_h as well as *tcp*.

2.1.2. Logistic TCP model

The phenomenological logistic TCP model is given by

$$\mathrm{TCP}(D) = \frac{1}{1+\exp\left\{4\gamma_{50}\left(1-\frac{D}{D_{50}}\right)\right\}}\,. \tag{15}$$

As before, we use the conditions and assumptions in Eqs. (3)-(6) to obtain for each of the N sub-volumes the model parameters in

$$\mathrm{TCP}_i(D) = \frac{1}{1+\exp\left\{4\gamma_{50,i}\left(1-\frac{D}{D_{50,i}}\right)\right\}}\,. \tag{16}$$

They are derived as

$$\gamma_{50,i} = B\,(D_\mathrm{h}+L_i)\,, \tag{17}$$

$$D_{50,i} = D_\mathrm{h}+L_i\,, \tag{18}$$

with the quantities $B=\gamma_{50,i}/D_{50,i}$ and L_i defined as,

$$B = \frac{\gamma_{50}}{D_{50}}\,\frac{1-tcp}{N-\sum_{j=1}^{N} tcp^{f_j}}\,, \tag{19}$$

$$L_i = \frac{1}{4B}\,\ln(tcp^{-f_i}-1)\,, \tag{20}$$

as explicitly shown in Appendix B. Note that, in contrast to the Poisson model, the parameters $\gamma_{50,i}$ and $D_{50,i}$ of the logistic model depend on the number of sub-volumes N as well as the dose level D_h (at which the f_i were determined) and the corresponding total TCP value, *tcp*.

2.2. Patient characteristics and dose planning

We applied the presented TCP modeling approach to 45 advanced stage head and neck cancer patients (T3 or T4; stages III to IV B) [24, 25]. They were included in a treatment planning study comparing a simultaneous integrated boost (SIB) dose escalation strategy delivered either with photon or proton irradiation as described in detail by Jakobi et *al.* [25] In brief, for each patient an intensity modulated radiotherapy (IMRT) and an intensity modulated proton therapy (IMPT) plan was prepared with the same planning goals. The target volume was divided into three sub-volumes. The gross tumor volume (GTV) comprised the bulky tumor volume and in the case of two patients with N3 stage additionally the lymph nodes. The clinical target volume (CTV) contained the GTV and involved lymph nodes (independent of the N stage) extended by a 5-10 mm margin. An elective CTV (CTVE)

was contoured according to the recommendations by Grégoire et *al.* [26]. A planning target volume (PTV) was created by adding a margin of 5 mm in cranio-caudal direction and 4 mm in plane. Total doses of 72 Gy and 79.8 Gy in 36 fractions (once every weekday) were prescribed to the CTV and GTV, respectively, with a 2.3 Gy SIB during the last 26 fractions. A dose level of 50 Gy within the first 25 fractions was prescribed to the CTVE. After 25 fractions, treatment plan adaptation was performed based on a second computed tomography scan. Throughout this work, proton dose values are products of physical dose and a constant factor of 1.1, which models the relative biological effectiveness of protons.

2.3. Dose response modeling

The considered patient dataset is exemplary for a target volume consisting of regions with different recurrence risk. Furthermore, the underlying treatment protocol uses a non-uniform dose prescription, i.e., the prescribed dose differed for the different target sub-volumes. In order to estimate the overall dose response we, therefore, divided the target volume in high-risk and low-risk sub-volumes given by the delineated GTV and the CTV structures, respectively. The low-risk volume was subdivided into the high-dose CTV and the elective CTVE. The total TCP for a patient is, according to Eq. (3), given by

$$\mathrm{TCP}_{\mathrm{patient}} = \mathrm{TCP}_{\mathrm{GTV}} \times \mathrm{TCP}_{\mathrm{CTV}} \times \mathrm{TCP}_{\mathrm{CTVE}} \,. \tag{21}$$

Note, clinically-defined contours often overlap (e.g., GTV and CTV). Since the derived modeling approach requires all target sub-volumes to be disjoint, inner sub-volumes are excluded from outer sub-volumes (e.g., here the GTV is excluded from the CTV). Here, we keep the same labeling for the resulting three disjoint sub-volumes. The normalized tumor dose (NTD) was obtained by correcting the fractionation effect compared to 2 Gy on a voxel basis using an α/β ratio of 10 Gy for all sub-volumes. We performed the TCP modeling in sub-volume i by applying a voxel-based Poisson model on the heterogeneous normalized tumor dose distribution, $\mathbf{NTD}_i$, in that sub-volume,

$$\mathrm{TCP}_i(\mathbf{NTD}_i) = \prod_j \mathrm{TCP}_i(NTD_{i,j})^{v_j} \,, \tag{22}$$

where $NTD_{i,j}$ and v_j are the normalized dose bins and the relative volumes of the differential dose-volume histogram (DVH), respectively, for sub-volume i. All TCP calculations were performed within the modeling framework of the recently developed tool for remote comparison of particle and photon plans (ReCompare) [27, 28]. The framework provides routines to calculate

differential DVHs for all contoured structures found in the photon and proton treatment plans. A voxel-based correction for fractionation effects can be selected. Different model functions, such as a logistic and a Poisson model are implemented as in [9] and are applied to the differential DVH to calculate the TCP according to Eq. (22).

As a comparison, we also determined TCP values for all patients using the simple modeling approach that assumes a homogeneous dose-response (i.e., the same clonogen cell density and radiosensitivity) in the whole target volume. The same parameters for overall control D_{50} and γ_{50} were employed as for the sub-volume modeling. To estimate the control of a target sub-volume, in this case, the sub-volume TCP had to be scaled,

$$\mathrm{TCP}_i = \mathrm{TCP}_i(\mathbf{NTD}_i; D_{50}, \gamma_{50})^{\frac{V_i}{V}} , \tag{23}$$

according to the size of sub-volume V_i relative to the total target volume V, i.e., proportional to the relative number of clonogen cells in V_i. This scaling ensures the same total TCP as estimated with the sub-volume model for a uniform dose coverage of the total target volume.

We chose TCP model parameters for local control, $D_{50} = 70.0$ Gy and $\gamma_{50} = 1.5$, within the range of radioresistant head and neck tumors [2] since all patients in the study cohort had a high tumor burden. Based on an analysis of the spatial distribution of recurrences in head and neck tumor patients by Due et *al.* [12], we estimated for all patients the same relative failure proportions of $f_{\mathrm{GTV}} = 0.82$ in the GTV and 0.18 in the surrounding clinical tumor volumes where $f_{\mathrm{CTV}} = 0.16$ was attributed to the non-elective volume alone.

Since notable uncertainties can be observed for TCP parameters, we performed a sensitivity analysis to quantify the dependence on the input parameters, namely, D_{50} and γ_{50} as well as f_{GTV} and f_{CTVE}. In each case, all but one input parameter were kept at constant values (70 Gy, 1.5, 0.80, and 0.02, respectively) while the remaining parameter was varied within a certain range: 60 Gy $\leq D_{50} \leq$ 80 Gy; $0.5 \leq \gamma_{50} \leq 3.0$; $0.5 \leq f_{\mathrm{GTV}} \leq 0.95$; and $0.0 \leq f_{\mathrm{CTV}} \leq 0.12$. The sum of all f_i remained unity by altering the proportion of failures in the CTV accordingly. For the TCP comparison of individual patients two-sided paired t-tests were used and p-values < 0.05 were considered significant.

3. Results

3.1. Properties of tumor sub-volume TCP model

The target volume was divided into three sub-volumes with different failure risks representing an inhomogeneous dose response. Model parameters

Table 1: Sub-volume TCP parameters for the Poisson and the logistic model assuming three target sub-volumes GTV, CTV, and CTVE with failure proportions $\mathbf{f} = [0.82, 0.16, 0.02]$. The parameters were obtained for three different *tcp* levels and the input parameters $D_{50} = 70$ Gy and $\gamma_{50} = 1.5$.

tcp	Parameter	GTV	CTV	CTVE
Poisson model				
	$D_{50,i}$	66.79	40.36	6.73
	$\gamma_{50,i}$	1.43	0.86	0.14
Logistic model				
0.3	$D_{50,i}$	67.29	38.78	8.96
	$\gamma_{50,i}$	1.22	0.70	0.16
0.6	$D_{50,i}$	66.52	43.78	17.19
	$\gamma_{50,i}$	1.32	0.87	0.34
0.9	$D_{50,i}$	67.13	47.34	22.61
	$\gamma_{50,i}$	1.42	1.00	0.48

for each sub-volume were obtained for the Poisson and the logistic model (Table 1). These TCP_i curves were compared to a standard TCP curve (homogeneous dose response in the target) with the same D_{50} and γ_{50} parameters (Fig. 2). In the case of the Poisson model, the product of all sub-volume TCP_i equals, at any homogeneous dose level D_h, the total TCP (Fig. 2a) and the parameters $D_{50,i}$ and $\gamma_{50,i}$ are independent of D_h. For the logistic model, the sub-volume TCP_i curves depend on D_h – i.e., the *tcp* level – at which the f_i were obtained (Figs. 2b-2d). Hence, the product $\prod_i \mathrm{TCP}_i$ of all sub-volume TCP_i differs from the standard TCP modeling curve. In general, this difference was small and vanished [due to the condition in Eq. (3)] around the dose level $D = D_\mathrm{h}$. At any homogeneous dose level D, the product $\prod_i \mathrm{TCP}_i(D)$ was smaller than or equal to the (clinically observed) $\mathrm{TCP}(D)$, based on homogeneous modeling making that product a conservative approximation. Some TCP_i curves for low-risk sub-volumes were nonzero at zero dose. This resembles the dose response for, e.g., elective clinical target volumes with control probability much greater than zero, even without radiotherapy [29].

Following the assumption in Eq. (6), the slope $\gamma_{50,i}/D_{50,i}$ at 50% TCP_i is for all sub-volume curves the same for a given set of input parameters (cf. Fig. 2). We studied the effect of this assumption by comparing it to an alternative approach, $\mathrm{TCP}_i^\mathrm{alt}$, that assumes instead $\gamma_{50,i}$ to be the same in all sub-volumes [21]. This alternative approach resulted in steep $\mathrm{TCP}_i^\mathrm{alt}$ curves for low $D_{50,i}$ and shallow $\mathrm{TCP}_i^\mathrm{alt}$ curves for high $D_{50,i}$ (not shown). For the logistic model, it yielded for vanishing dose ($D \to 0$) the same $\mathrm{TCP}_i^\mathrm{alt}(0)$ value for all i. The total TCP for the alternative assumption, $\prod_i \mathrm{TCP}_i^\mathrm{alt}$,

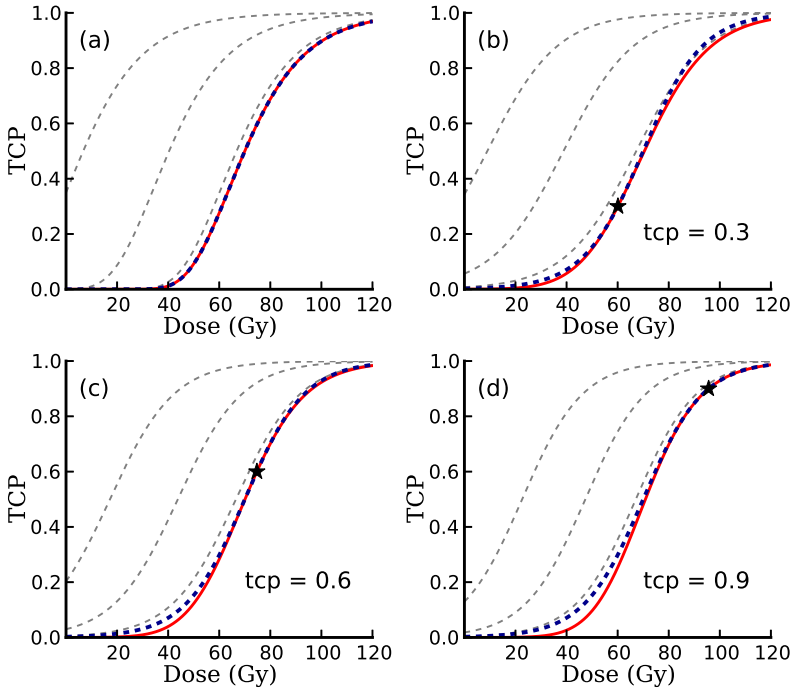

Figure 2: Tumor control probability (TCP) as function of homogeneous tumor dose. A standard TCP curve (homogeneous dose response) is compared with TCP curves for the sub-volume model with three sub-volumes (model parameters in Table 1): (a) Poisson model; logistic model with failure patterns (i.e., f_i) determined at (b) $tcp = 0.3$, (c) $tcp = 0.6$, and (d) $tcp = 0.9$ (indicated by stars). Solid red line, product of sub-volume TCP_i; dashed blue line, standard total TCP; dashed grey lines, sub-volume TCP_i curves with increasing f_i values from left to right.

was similar to that for the presented approach, $\prod_i \mathrm{TCP}_i$. Quantitatively, however, $\prod_i \mathrm{TCP}_i^{\mathrm{alt}}$ was for all homogeneous dose levels, D, either smaller than or equal to $\prod_i \mathrm{TCP}_i$ and we get the inequality,

$$\mathrm{TCP}(D) \geq \prod_i \mathrm{TCP}_i(D) \geq \prod_i \mathrm{TCP}_i^{\mathrm{alt}}(D)\,. \tag{24}$$

Therefore, our assumption in Eq. (6) was superior in reproducing the clinically obtained overall dose response curve $\mathrm{TCP}(D)$ that served as input.

3.2. TCP estimates for inhomogeneous photon and proton treatment plans

The presented sub-volume approach based on the Poisson model (model parameters in Table 1) was used to estimate local control for photon (X) and proton (P) treatment plans of 45 head and neck cancer patients. The modeled mean total TCP values (± standard deviation) for photon plans,

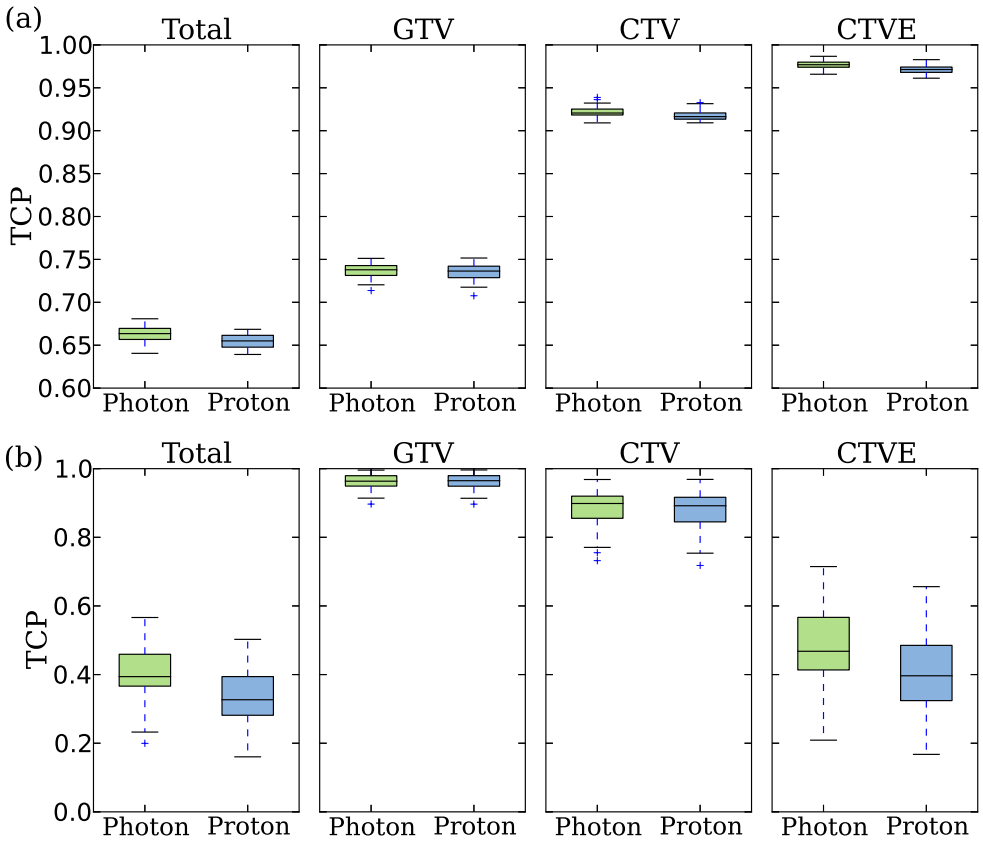

Figure 3: Distribution of tumor control probability (TCP) values of photon and proton treatment plans for 45 head and neck cancer patients: TCP for total target volume (product of all sub-volume TCP) and for disjoint sub-volumes GTV, CTV, and CTVE. (a) Inhomogeneous dose response using the sub-volume model; (b) assuming homogeneous dose response in the target volume. Note the different scales.

66.3 (±0.9) %, and proton plans, 65.5 (±0.8) %, as well as those for the disjoint GTV, CTV, and CTVE sub-volumes (Fig. 3a) differed by less than a percent (Table 2). While these differences were statistically significant they appeared too small to be clinically relevant. They originated from systematically higher than prescribed mean dose levels for photon plans in the CTV and CTVE, while proton irradiation allowed for better dose conformity with mean doses closer to the prescription. Mean DVH curves for proton and photon plans, based on all 45 patients (Fig. 4), were very similar for the GTV. The systematically elevated dose (on average 4.9%) for photon plans in the CTVE resulted in the small mean difference $\Delta\mathrm{TCP}_{\mathrm{X-P,\,CTVE}}$ of 0.6% points and thereby contributed predominantly to the small difference in total TCP between photon and proton plans.

Table 2: Mean tumor control probabilities (TCP) and standard deviations (σ) for photon (X) and proton (P) plans of 45 head and neck cancer patients: TCP estimates for the total target volume (product of all sub-volume TCP) and for the disjoint sub-volumes GTV, CTV, and CTVE employing the sub-volume model.

Plan	D_{pre} [Gy]	TCP ($\pm\sigma$) [%]	$\Delta\mathrm{TCP}_{\mathrm{X-P}}$	p-value
TCP total				
Photon		66.3 ($\pm$0.9)	0.8	< 0.001
Proton		65.5 ($\pm$0.8)		
TCP GTV				
Photon	79.8	73.7 ($\pm$0.8)	0.2	0.007
Proton	79.8	73.5 ($\pm$0.9)		
TCP CTV				
Photon	72.0	92.2 ($\pm$0.6)	0.5	< 0.001
Proton	72.0	91.7 ($\pm$0.5)		
TCP CTVE				
Photon	50.0	97.7 ($\pm$0.4)	0.6	< 0.001
Proton	50.0	97.1 ($\pm$0.5)		

$\Delta\mathrm{TCP}_{\mathrm{X-P}}$: TCP difference: Photon - Proton.
D_{pre}: prescribed dose.

In contrast, TCP modeling assuming a homogeneous dose response within the entire target volume – as frequently employed for TCP modeling – and using as input the same D_{50} and γ_{50} parameters lead to completely different results (Fig. 3b). The total TCP values (mean photon: 39.6 ($\pm$8.2) %, mean proton: 32.9 ($\pm$8.1) %) decreased by more than 25% points compared to the sub-volume model approach and differed by on average 6.7% points between photon and proton plans. The large difference to the estimates with the sub-volume TCP approach stemmed mainly from the much lower (about 50% points) calculated control probability in the CTVE, where the lower radiation dose prescribed to the CTVE was decisive. Also, the TCP_i values within the other two sub-volumes changed with respect to the sub-volume model approach and the variance of all TCP distributions increased markedly.

The discussed total TCP values (i.e., the product of sub-volume TCP_i) varied substantially with the input parameters γ_{50}, D_{50} but in a less pronounced fashion with the distribution of failures f_i (Fig. 5). For example, even a fivefold increase in proportional failure risk in the low-dose sub-volume CTVE [Fig. 5d)] resulted only in a decrease in total TCP by 3.5% points. The TCP difference between the two treatment modalities photons and protons appeared fairly robust against variations of these parameters and was greatest for large γ_{50} and f_{CTVE} values.

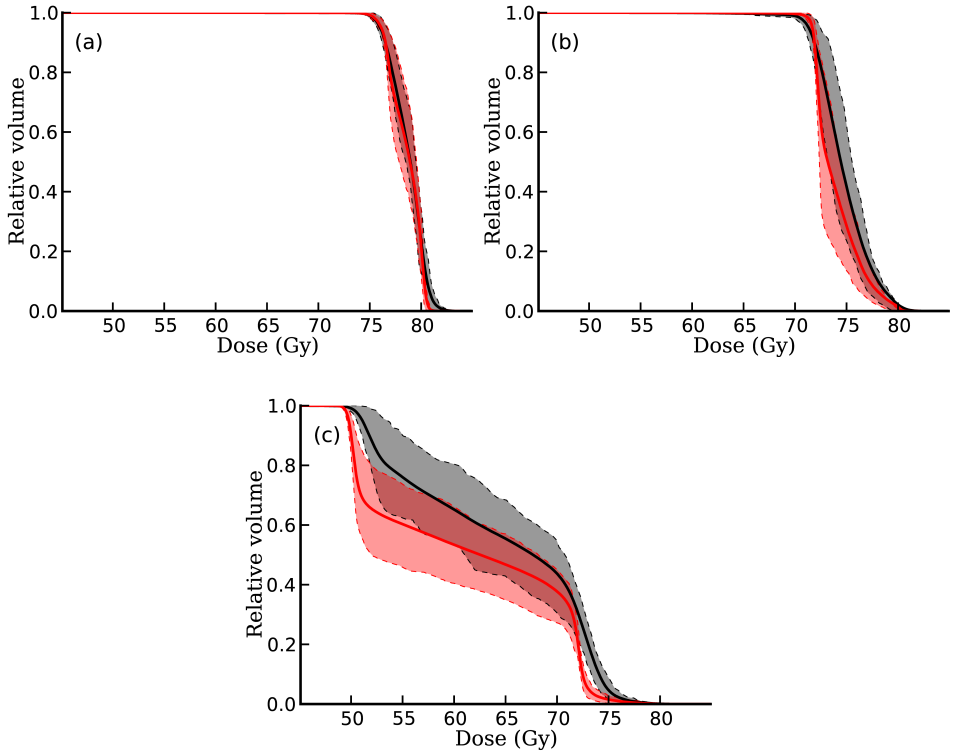

Figure 4: Mean dose volume histogram for treatment plans of 45 head and neck cancer patients with one standard deviation as shaded area: red lines, proton plans and black lines, photon plans. Disjoint target sub-volumes: (a) GTV, (b) CTV, and (c) CTVE.

4. Discussion

The derived formalism describes TCP modeling for target volumes with spatially varying risk of failure. It is based on the empirically accessible parameters D_{50} and γ_{50} for the total TCP and the observed proportion of failures, f_i, in each considered target sub-volume. Thereby, it allows for a convenient calculation of the TCP for spatially inhomogeneous target doses or potentially optimizing inhomogeneous dose prescriptions (e.g., dose boost strategies) to counteract the inhomogeneous dose response given the availability of reliable data on the failure risk.

The same (inhomogeneous) dose prescription for 45 head and neck cancer patients applied either by photon or proton treatment resulted in very similar TCP estimates (using the sub-volume modeling), despite notably higher doses for photon irradiation in the low-risk tumor sub-volumes compared to proton treatment plans. While the absolute TCP values strongly depend on D_{50} and γ_{50}, the TCP differences between photon an proton plans appear to be robust. In general, the proton plans exhibit more conformal and thereby

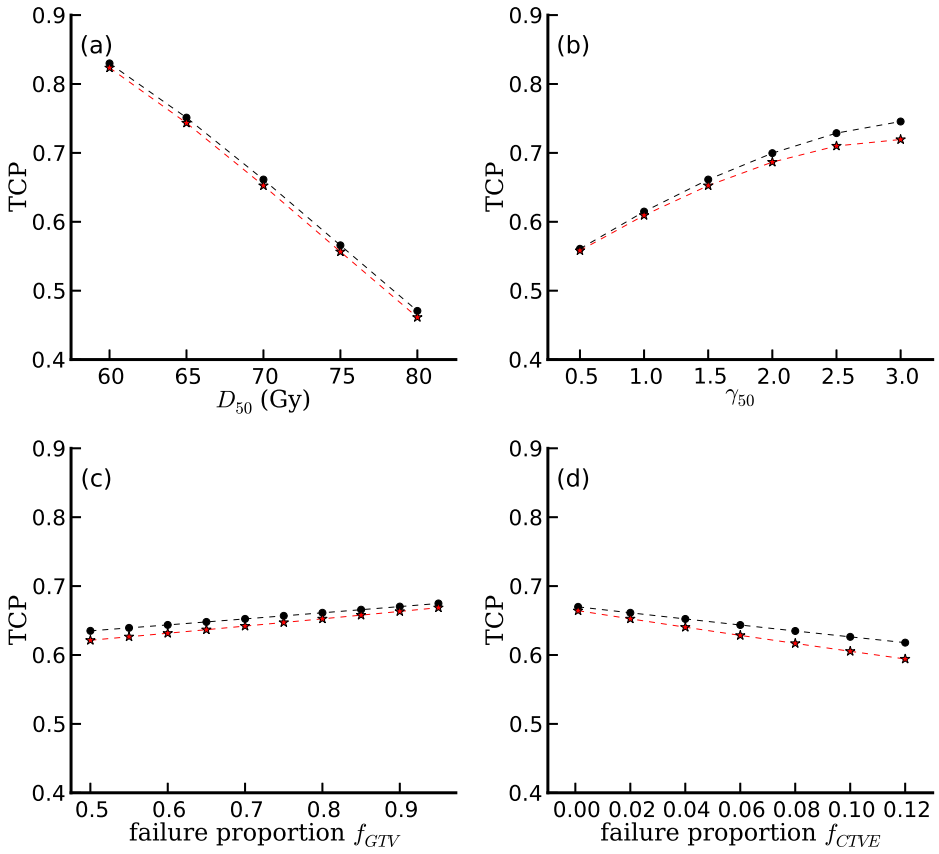

Figure 5: Mean tumor control probability (TCP) values for treatment plans of 45 head and neck cancer patients using the sub-volume model: red stars, proton plans and black circles, photon plans. Variation of TCP as a function of the input parameters (a) D_{50}, (b) γ_{50}, and proportion of failures f in the (c) GTV and (d) CTVE.

lower dose levels in the outer target sub-volumes as well as in the surrounding normal tissue. The improved conformity results from the inverse depth-dose profile of proton beams: the dose increases with penetration depth in the patient until the Bragg peak – which can be placed inside the target volume – and drops steeply to zero afterward. In contrast to the similar TCP, estimated normal tissue complication probabilities (NTCP) for these plans were found to be significantly higher for individual patients in the case of photon plans, depending on patient geometry and endpoint [25, 30].

Assumption of a homogeneous dose response (i.e., homogeneous clonogen cell density and radiosensitivity) in the entire target volume is an inappropriate modeling strategy for the current plan evaluation. It results in substantially different TCP estimates: a low probability of local failures in the GTV and most failures in the low-risk CTVE. These estimates clearly contradict

clinically observed data, which demonstrate that the vast majority of failures occur in-field [14–17]. The exceptionally high modeled failure probability in the CTVE results from the assumed uniform clonogen density everywhere in the target volume that leads, together with the relatively large CTVE volume, to an estimated large number of clonogen cells and therefore to small TCP values. Such inappropriate TCP modeling outcomes occur for all tumor entities with spatially inhomogeneous dose response and demonstrate the need for good estimates of the dose-response parameters $D_{50,i}$ and $\gamma_{50,i}$ in target sub-volumes. Accordingly, to some degree (simple) sub-volume modeling has been employed earlier, e.g., by separately estimating the TCP of elective lymph node volumes, especially, for head and neck cancers [2, 21, 29]. The derived sub-volume TCP modeling could be described as a generalization of such simple two-level TCP approaches supporting technically an arbitrary number of different dose-response levels in one target volume.

An assumption of the current approach is the independence of failure between each target sub-volume [Eq. (3)]. However, currently available clinical data do not allow for the exclusion of this assumption, as discussed in [21]. While regional similarities within tumors are well established, their extent might be tumor-dependent and overlapping, as found in molecular-imaging studies in canine patients [31, 32]. Prospectively, clinical trials employing optimized dose distributions may serve as an indicator by considering whether more failures will be observed in the (de-escalated) periphery than expected. In this context, the proposed method may help to quantify this hypothesis in order to falsify or to validate the underlying assumption. In this context, it is important to interpret the low $D_{50,i}$ values in the CTVE as population risk estimates for rare events. For those rare individuals with recurrence in this region, a sufficiently high dose must still be delivered to control tumor growth. Unreflected use in objective functions to plan individual treatments may lead to severe under-dosage of the elective volumes. The approach to relate the total TCP via the proportion of failures f_i in a sub-volume to the corresponding TCP_i [Eq. (5)] is consistent for the Poisson model. For the logistic model this is formally not the case. However, for all studied situations numerical discrepancies regarding the self-consistency were found to be small.

The derived approach assumes the same slope $\gamma_{50,i}/D_{50,i}$ of the TCP_i in all sub-volumes [Eq. (6)]. When compared to the technique of assuming that $\gamma_{50,i}$ is the same for all i, the former assumption is superior in reproducing the clinically observed total TCP. When relating the TCP with the clonogen surviving fraction S_c and clonogen cell number N_c in the usual way with Poisson statistics [33] ($\mathrm{TCP} = \exp\left[-N_\mathrm{c}\, S_\mathrm{c}\right]$), the same slope $\gamma_{50,i}/D_{50,i}$ for all i complies with a uniform dose response S_c throughout the target volume [34].

Then, the proportion of failures f_i would conceptually depend on the clonogen cell number $N_{c,i}$ in sub-volume i and the clonogen cell density (CCD) would be expected to be lower in low-risk sub-volumes with small f_i such as the CTVE. The alternative assumption, namely, the same $\gamma_{50,i}$ for all i would suggest more radio-resistant cells in the high-risk regions. These descriptions are likely to be simplifications and accurate values for radiosensitivity and number of tumor stem cells are difficult to obtain for an individual patient. However, the strength of the derived sub-volume TCP approach is exactly that detailed knowledge of such data is not required. Some prior work on modeling different recurrence risks within the CTV and GTV based on the linear quadratic model has been done by varying the CCD in the case of lung irradiation [35]. A shortcoming of such an approach is the fact that clinical data on the CCD in the microscopic extension around the GTV are not available. In contrast, the present approach allows for a simpler and mathematically more stable empirical fit to the spatial patterns of clinical recurrence data.

The reliability of any modeling approach relies on the accuracy of the input parameters. The sensitivity analysis pointed out that confidence intervals for total TCP estimates are predominantly driven by the uncertainty of the established total TCP parameters D_{50} and γ_{50} (which can be on the order of $\pm 20\%$) and much less by the precise distribution of failures within the target volume. For several tumor entities, a dependence of TCP on the volume of the tumor has been observed (e.g., head and neck [36] and lung [37, 38]). This volume dependence can be included in the method in a straightforward way by allowing the total TCP (i.e., D_{50}, γ_{50}) to depend on the tumor volume. In the current work and elsewhere [30, 39], the derived approach was applied to dose distributions from plan comparison studies to obtain TCP estimates. Such applications do not serve as a verification of the approach. Instead, a (prospective) clinical study – potentially with an inhomogeneous dose prescription – could be used.

The sub-volume TCP approach may be beneficial when designing clinical trials that aim at testing the impact of dose escalation of high-risk (and de-escalation of low-risk) tumor sub-volumes based on the well established clinical experience from homogeneous dose irradiation. It does not require particular knowledge of underlying radiobiologic parameters. The presented formulation allows for convenient optimization of the dose prescription and for estimating patient numbers. Potentially, even individualized inhomogeneous dose distributions could be designed, provided that reliable patient-specific information on the expected failure pattern would eventually become available.

5. Conclusion

We derived a tumor control probability modeling approach for spatially inhomogeneous risk of failure. The method presented is valuable for three reasons: (a) it is based on empirical outcome data; (b) it can be applied for inhomogeneous tumor dose (boost strategies) and different tumor entities as well as dose-response models; and (c) it is presented in a convenient analytical form. In contrast, standard modeling (assuming spatially homogeneous failure risk) may lead to clinically unexpected failure distributions for inhomogeneous dose prescriptions: the lowest tumor control in the low-risk elective volume. The presented approach is able to target clinically observed spatial patterns of local failures by redistributing the prescribed dose to decrease the expected total risk of failures in a patient cohort. Its predictive power depends on the uncertainty of the input data: established tumor control parameters D_{50} and γ_{50} and to a smaller extent empirical pattern of failure risk.

Acknowledgments

The authors are grateful to Howard Thames for intensive discussions on the sub-volume TCP modeling approach and Damian McLeod for reading the manuscript.

References

[1] H. Holthusen, Erfahrungen über die Verträglichkeitsgrenze von Röntgenstrahlen und deren Nutzanwendung, Strahlentherapie 57 (1936) 254–69.

[2] P. Okunieff, D. Morgan, A. Niemierko, H. D. Suit, Radiation dose-response of human tumors, International Journal of Radiation Oncology*Biology*Physics 32 (4) (1995) 1227–1237. doi:10.1016/0360-3016(94)00475-Z.
URL http://www.sciencedirect.com/science/article/pii/0360301694004752

[3] J. D. Fenwick, Predicting the radiation control probability of heterogeneous tumour ensembles: data analysis and parameter estimation using a closed-form expression, Physics in Medicine and Biology 43 (8) (1998) 2159. doi:10.1088/0031-9155/43/8/012.
URL http://iopscience.iop.org/0031-9155/43/8/012

[4] J. Willner, K. Baier, L. Pfreundner, M. Flentje, Tumor Volume and Local Control in Primary Radiotherapy of Nasopharyngeal Carcinoma, Acta Oncologica 38 (8) (1999) 1025–1030. doi:10.1080/028418699432301.
URL http://dx.doi.org/10.1080/028418699432301

[5] S. M. Bentzen, S. L. Tucker, Quantifying the position and steepness of radiation dose-response curves, International Journal of Radiation Biology 71 (5) (1997) 531–542. doi:10.1080/095530097143860.
URL http://informahealthcare.com/doi/abs/10.1080/095530097143860

[6] S. M. Bentzen, P. M. Harari, W. A. Tom, M. P. Mehta, Radiation Oncology Advances - Springer, Springer, 2008.
URL http://link.springer.com/book/10.1007/978-0-387-36744-6

[7] N. Stavreva, P. Stavrev, B. Warkentin, B. G. Fallone, Derivation of the expressions for 50 and D50 for different individual TCP and NTCP models, Physics in Medicine and Biology 47 (20) (2002) 3591. doi:10.1088/0031-9155/47/20/303.
URL http://iopscience.iop.org/0031-9155/47/20/303

[8] Y. Kim, W. A. Tomé, Risk-adaptive optimization: Selective boosting of high-risk tumor subvolumes, International Journal of Radiation Oncology*Biology*Physics 66 (5) (2006) 1528–1542. doi:10.1016/j.ijrobp.2006.08.032.
URL http://www.sciencedirect.com/science/article/pii/S0360301606027933

[9] B. Warkentin, P. Stavrev, N. Stavreva, C. Field, B. G. Fallone, A TCP-NTCP estimation module using DVHs and known radiobiological models and parameter sets, J Appl Clin Med Phys 5 (1) (2004) 50–63.

[10] M. Joiner, A. v. d. Kogel, Basic Clinical Radiobiology Fourth Edition, Hodder Education, 2009.

[11] A. K. Due, I. R. Vogelius, M. C. Aznar, S. M. Bentzen, A. K. Berthelsen, S. S. Korreman, C. A. Kristensen, L. Specht, Methods for estimating the site of origin of locoregional recurrence in head and neck squamous cell carcinoma, Strahlenther Onkol 188 (8) (2012) 671–676. doi:10.1007/s00066-012-0127-y.

URL http://link.springer.com/article/10.1007/s00066-012-0127-y

[12] A. K. Due, I. R. Vogelius, M. C. Aznar, S. M. Bentzen, A. K. Berthelsen, S. S. Korreman, A. Loft, C. A. Kristensen, L. Specht, Recurrences after intensity modulated radiotherapy for head and neck squamous cell carcinoma more likely to originate from regions with high baseline [18F]-FDG uptake, Radiotherapy and Oncology 111 (3) (2014) 360–365. doi:10.1016/j.radonc.2014.06.001.
URL http://www.sciencedirect.com/science/article/pii/S0167814014002242

[13] A. Abramyuk, S. Tokalov, K. Zöphel, A. Koch, K. Szluha Lazanyi, C. Gillham, T. Herrmann, N. Abolmaali, Is pre-therapeutical FDG-PET/CT capable to detect high risk tumor subvolumes responsible for local failure in non-small cell lung cancer?, Radiotherapy and Oncology 91 (3) (2009) 399–404. doi:10.1016/j.radonc.2009.01.003.
URL http://www.sciencedirect.com/science/article/pii/S0167814009000085

[14] F. De Felice, C. Thomas, S. Barrington, A. Pathmanathan, M. Lei, T. G. Urbano, Analysis of loco-regional failures in head and neck cancer after radical radiation therapy, Oral Oncology 51 (11) (2015) 1051–1055. doi:10.1016/j.oraloncology.2015.08.004.
URL http://www.sciencedirect.com/science/article/pii/S1368837515002948

[15] A. S. Garden, L. Dong, W. H. Morrison, E. M. Stugis, B. S. Glisson, S. J. Frank, B. M. Beadle, G. B. Gunn, D. L. Schwartz, M. S. Kies, R. S. Weber, K. K. Ang, D. I. Rosenthal, Patterns of Disease Recurrence Following Treatment of Oropharyngeal Cancer With Intensity Modulated Radiation Therapy, International Journal of Radiation Oncology*Biology*Physics 85 (4) (2013) 941–947. doi:10.1016/j.ijrobp.2012.08.004.
URL http://www.sciencedirect.com/science/article/pii/S0360301612033901

[16] G. Studer, U. M. Luetolf, C. Glanzmann, Locoregional failure analysis in head-and-neck cancer patients treated with IMRT, Strahlentherapie und Onkologie 183 (8) (2007) 417–423. doi:10.1007/s00066-007-1663-8.
URL http://link.springer.com/article/10.1007/s00066-007-1663-8

[17] K. S. C. Chao, G. Ozyigit, B. N. Tran, M. Cengiz, J. F. Dempsey, D. A. Low, Patterns of failure in patients receiving definitive and postoperative IMRT for head-and-neck cancer, International Journal of Radiation Oncology*Biology*Physics 55 (2) (2003) 312–321. doi:10.1016/S0360-3016(02)03940-8.
URL http://www.sciencedirect.com/science/article/pii/S0360301602039408

[18] D. Thorwarth, X. Geets, M. Paiusco, Physical radiotherapy treatment planning based on functional PET/CT data, Radiotherapy and Oncology 96 (3) (2010) 317–324. doi:10.1016/j.radonc.2010.07.012.
URL http://www.sciencedirect.com/science/article/pii/S0167814010004032

[19] K. Hendrickson, M. Phillips, W. Smith, L. Peterson, K. Krohn, J. Rajendran, Hypoxia imaging with [F-18] FMISO-PET in head and neck cancer: Potential for guiding intensity modulated radiation therapy in overcoming hypoxia-induced treatment resistance, Radiotherapy and Oncology 101 (3) (2011) 369–375. doi:10.1016/j.radonc.2011.07.029.
URL http://www.sciencedirect.com/science/article/pii/S0167814011004075

[20] W. van Elmpt, D. De Ruysscher, A. van der Salm, A. Lakeman, J. van der Stoep, D. Emans, E. Damen, M. Öllers, J.-J. Sonke, J. Belderbos, The PET-boost randomised phase II dose-escalation trial in non-small cell lung cancer, Radiotherapy and Oncology 104 (1) (2012) 67–71. doi:10.1016/j.radonc.2012.03.005.
URL http://www.sciencedirect.com/science/article/pii/S0167814012001181

[21] I. R. Vogelius, K. Håkansson, A. K. Due, M. C. Aznar, A. K. Berthelsen, C. A. Kristensen, J. Rasmussen, L. Specht, S. M. Bentzen, Failure-probability driven dose painting, Med Phys 40 (8) (2013) 081717. doi:10.1118/1.4816308.

[22] S. F. Petit, H. J. W. L. Aerts, J. G. M. van Loon, C. Offermann, R. Houben, B. Winkens, M. C. Öllers, P. Lambin, D. De Ruysscher, A. L. A. J. Dekker, Metabolic control probability in tumour subvolumes or how to guide tumour dose redistribution in non-small cell lung cancer (NSCLC): An exploratory clinical study, Radiotherapy and Oncology 91 (3) (2009) 393–398. doi:10.1016/j.radonc.2009.02.020.
URL http://www.sciencedirect.com/science/article/pii/S0167814009000887

[23] D. Thorwarth, M. Notohamiprodjo, D. Zips, A.-C. Müller, Personalized precision radiotherapy by integration of multi-parametric functional and biological imaging in prostate cancer: A feasibility study, Zeitschrift für Medizinische Physik in press. doi:10.1016/j.zemedi.2016.02.002.
URL http://www.sciencedirect.com/science/article/pii/S0939388916000222

[24] D. Zips, K. Zöphel, N. Abolmaali, R. Perrin, A. Abramyuk, R. Haase, S. Appold, J. Steinbach, J. Kotzerke, M. Baumann, Exploratory prospective trial of hypoxia-specific PET imaging during radiochemotherapy in patients with locally advanced head-and-neck cancer, Radiother Oncol 105 (1) (2012) 21–28. doi:10.1016/j.radonc.2012.08.019.

[25] A. Jakobi, A. Bandurska-Luque, K. Stützer, R. Haase, S. Löck, L.-J. Wack, D. Mönnich, D. Thorwarth, D. Perez, A. Lühr, D. Zips, M. Krause, M. Baumann, R. Perrin, C. Richter, Identification of Patient Benefit From Proton Therapy for Advanced Head and Neck Cancer Patients Based on Individual and Subgroup Normal Tissue Complication Probability Analysis, International Journal of Radiation Oncology*Biology*Physics 92 (5) (2015) 1165–1174. doi:10.1016/j.ijrobp.2015.04.031.
URL http://www.sciencedirect.com/science/article/pii/S0360301615004319

[26] V. Grégoire, E. E. Coche, G. Cosnard, M. Hamoir, H. Reychler, Selection and delineation of lymph node target volumes in head and neck conformal and intensity modulated radiation therapy, in: V. Grgoire, P. Scalliet, K. K. Ang (Eds.), Clinical Target Volumes in Conformal and Intensity Modulated Radiation Therapy, Medical Radiology, Springer Berlin Heidelberg, 2004, pp. 69–90.
URL http://link.springer.com/10.1007/978-3-662-06270-8

[27] A. Lühr, S. Löck, K. Roth, S. Helmbrecht, A. Jakobi, J. B. Petersen, U. Just, M. Krause, W. Enghardt, M. Baumann, Concept for individualized patient allocation: ReCompare–remote comparison of particle and photon treatment plans, Radiat. Oncol. 9 (1) (2014) 59. doi:10.1186/1748-717X-9-59.
URL http://www.ro-journal.com/content/9/1/59/abstract

[28] S. Löck, K. Roth, T. Skripcak, M. Worbs, S. Helmbrecht, A. Jakobi, U. Just, M. Krause, M. Baumann, W. Enghardt, A. Lühr, Implementation of a software for REmote COMparison of PARticlE and

photon treatment plans: ReCompare, Zeitschrift für Medizinische Physikdoi:10.1016/j.zemedi.2015.02.001.
URL http://www.sciencedirect.com/science/article/pii/S0939388915000197

[29] A. Eisbruch, R. L. Foote, B. O'Sullivan, J. J. Beitler, B. Vikram, Intensity-modulated radiation therapy for head and neck cancer: Emphasis on the selection and delineation of the targets, Seminars in Radiation Oncology 12 (3) (2002) 238–249. doi:10.1053/srao.2002.32435.
URL http://www.sciencedirect.com/science/article/pii/S1053429602800649

[30] A. Jakobi, K. Stützer, A. Bandurska-Luque, S. Löck, R. Haase, L.-J. Wack, D. Mönnich, D. Thorwarth, D. Perez, A. Lühr, D. Zips, M. Krause, M. Baumann, R. Perrin, C. Richter, NTCP reduction for advanced head and neck cancer patients using proton therapy for complete or sequential boost treatment versus photon therapy, Acta Oncologica 54 (9) (2015) 1658–1664. doi:10.3109/0284186X.2015.1071920.
URL http://dx.doi.org/10.3109/0284186X.2015.1071920

[31] S. R. Bowen, R. J. Chappell, S. M. Bentzen, M. A. Deveau, L. J. Forrest, R. Jeraj, Spatially resolved regression analysis of pre-treatment FDG, FLT and Cu-ATSM PET from post-treatment FDG PET: An exploratory study, Radiotherapy and Oncology 105 (1) (2012) 41–48. doi:10.1016/j.radonc.2012.05.002.
URL http://www.sciencedirect.com/science/article/pii/S0167814012002319

[32] T. Bradshaw, R. Fu, S. Bowen, J. Zhu, L. Forrest, R. Jeraj, Predicting location of recurrence using FDG, FLT, and Cu-ATSM PET in canine sinonasal tumors treated with radiotherapy, Physics in Medicine and Biology 60 (13) (2015) 5211. doi:10.1088/0031-9155/60/13/5211.
URL http://stacks.iop.org/0031-9155/60/i=13/a=5211

[33] T. R. Munro, C. W. Gilbert, The Relation Between Tumour Lethal Doses and the Radiosensitivity of Tumour Cells, Br. J. Radiol. 34 (400) (1961) 246–251. doi:10.1259/0007-1285-34-400-246.
URL http://www.birpublications.org/doi/abs/10.1259/0007-1285-34-400-246

[34] P. Stavrev, N. Stavreva, A. Niemierko, M. Goitein, Generalization of a model of tissue response to radiation based on the idea of functional subunits and binomial statistics, Phys. Med. Biol. 46 (5) (2001) 1501.

doi:10.1088/0031-9155/46/5/312.
URL http://iopscience.iop.org/0031-9155/46/5/312

[35] M. Guckenberger, A. Richter, J. Wilbert, M. Flentje, M. Partridge, Adaptive Radiotherapy for Locally Advanced NonSmall-Cell Lung Cancer Does Not Underdose the Microscopic Disease and has the Potential to Increase Tumor Control, International Journal of Radiation Oncology*Biology*Physics 81 (4) (2011) e275–e282. doi:10.1016/j.ijrobp.2011.01.067.
URL http://www.sciencedirect.com/science/article/pii/S0360301611002549

[36] T. Rutkowski, The role of tumor volume in radiotherapy of patients with head and neck cancer, Radiation Oncology 9 (1) (2014) 23. doi:10.1186/1748-717X-9-23.
URL http://www.ro-journal.com/content/9/1/23/abstract

[37] M. K. Martel, R. K. Ten Haken, M. B. Hazuka, M. L. Kessler, M. Strawderman, A. T. Turrisi, T. S. Lawrence, B. A. Fraass, A. S. Lichter, Estimation of tumor control probability model parameters from 3-D dose distributions of non-small cell lung cancer patients, Lung Cancer 24 (1) (1999) 31–37. doi:10.1016/S0169-5002(99)00019-7.
URL http://www.sciencedirect.com/science/article/pii/S0169500299000197

[38] M. Partridge, M. Ramos, A. Sardaro, M. Brada, Dose escalation for non-small cell lung cancer: Analysis and modelling of published literature, Radiotherapy and Oncology 99 (1) (2011) 6–11. doi:10.1016/j.radonc.2011.02.014.
URL http://www.sciencedirect.com/science/article/pii/S0167814011001095

[39] A. Jakobi, A. Lühr, K. Stützer, A. Bandurska-Luque, S. Löck, M. Krause, M. Baumann, R. Perrin, C. Richter, Increase in tumor control and normal tissue complication probabilities in advanced head-and-neck cancer for dose-escalated intensity-modulated photon and proton therapy, Frontiers in Oncology 5 (2015) 256. doi:10.3389/fonc.2015.00256.
URL http://journal.frontiersin.org/article/10.3389/fonc.2015.00256/full

Appendix A. Derivation of model parameters: Poisson model

The Poisson model for the total tumor,

$$\mathrm{TCP}(D) = \exp\left[\ln\left(\frac{1}{2}\right)\exp\left\{\frac{2\gamma_{50}}{\ln(2)}\left(1-\frac{D}{D_{50}}\right)\right\}\right], \tag{25}$$

is defined by the two model parameters D_{50} and γ_{50}. The proportion of failures f_i in each of the N tumor sub-volumes were obtained at the homogeneous dose D_h at which the total TCP is given by the short notation

$$tcp = \mathrm{TCP}(D_\mathrm{h})\,. \tag{26}$$

To fully describe the N sub-volume TCP_i curves,

$$\mathrm{TCP}_i(D) = \exp\left[\ln\left(\frac{1}{2}\right)\exp\left\{\frac{2\gamma_{50,i}}{\ln(2)}\left(1-\frac{D}{D_{50,i}}\right)\right\}\right], \tag{27}$$

we derive the N pairs of model parameters $\gamma_{50,i}$ and $D_{50,i}$ under the condition that the assumptions specified in Eqs. (3)-(6) are fulfilled. Accordingly, we need the first derivative of TCP with respect to dose

$$\begin{aligned}\frac{\mathrm{d}}{\mathrm{d}D}\mathrm{TCP}(D) &= \mathrm{TCP}(D)\underbrace{\ln\left(\frac{1}{2}\right)\exp\left\{\frac{2\gamma_{50}}{\ln(2)}\left(1-\frac{D}{D_{50}}\right)\right\}}_{=\ln(\mathrm{TCP}(D))}\frac{2\gamma_{50}}{\ln(2)}\left(-\frac{1}{D_{50}}\right) &(28)\\ &= -\mathrm{TCP}(D)\ln(\mathrm{TCP}(D))\,\frac{2}{\ln(2)}\,\frac{\gamma_{50}}{D_{50}}\,. &(29)\end{aligned}$$

Evaluated at the dose D_h and using Eq. (26) this results for the total tumor and the sub-volume i, respectively, in

$$\begin{aligned}\left.\frac{\mathrm{d}}{\mathrm{d}D}\mathrm{TCP}(D)\right|_{D_\mathrm{h}} &= -\frac{2}{\ln(2)}\,tcp\ln(tcp)\,\frac{\gamma_{50}}{D_{50}} &(30)\\ \left.\frac{\mathrm{d}}{\mathrm{d}D}\mathrm{TCP}_i(D)\right|_{D_\mathrm{h}} &= -\frac{2}{\ln(2)}\,tcp^{f_i}\,\ln(tcp)f_i\,A\,, &(31)\end{aligned}$$

where we used that according to Eq. (6) $A = \frac{\gamma_{50,i}}{D_{50,i}}$ is a constant independent of i. To determine A we first simplify the right hand side of Eq. (4),

$$\left.\frac{\mathrm{d}}{\mathrm{d}D}\mathrm{TCP}(D)\right|_{D_\mathrm{h}} = \sum_{i=1}^{N}\underbrace{\prod_{j=1}^{N}}_{i\neq j}\mathrm{TCP}_j(D_\mathrm{h})\left.\frac{\mathrm{d}}{\mathrm{d}D}\mathrm{TCP}_i(D)\right|_{D_\mathrm{h}} \tag{32}$$

$$= -\sum_{i=1}^{N} \underbrace{\prod_{j=1}^{N}}_{i\neq j} tcp^{f_j} \, \frac{2}{\ln(2)} \, tcp^{f_i} \, \ln(tcp) f_i \, A \tag{33}$$

$$= -\frac{2}{\ln(2)} \, A \sum_{i=1}^{N} \underbrace{tcp^{1-f_i} \, tcp^{f_i}}_{=tcp} \, \ln(tcp) f_i \tag{34}$$

$$= -\frac{2}{\ln(2)} \, A \, tcp \, \ln(tcp) \underbrace{\sum_{i=1}^{N} f_i}_{=1} \tag{35}$$

$$= -\frac{2}{\ln(2)} \, A \, tcp \, \ln(tcp) \, , \tag{36}$$

set it equal to the according left hand side as given in Eq. (30),

$$-\frac{2}{\ln(2)} \, \frac{\gamma_{50}}{D_{50}} \, tcp \, \ln(tcp) \;\; = \;\; -\frac{2}{\ln(2)} \, A \, tcp \, \ln(tcp) \, , \tag{37}$$

and obtain the simple relation,

$$A = \frac{\gamma_{50}}{D_{50}} \, , \tag{38}$$

which is independent of $D_{\rm h}$ and tcp.

To determine $\gamma_{50,i}$ and $D_{50,i}$ we use the definition of TCP_i in Eq. (27) at the dose $D_{\rm h}$ and employ the two relations previously given in Eqs. (5) and (38),

$$tcp^{f_i} = \exp\left[\ln\left(\frac{1}{2}\right) \exp\left\{\frac{2}{\ln(2)} \, (\gamma_{50,i} - D_{\rm h} \, A)\right\}\right] \tag{39}$$

$$= \exp\left[\ln\left(\frac{1}{2}\right) \exp\left\{\frac{2}{\ln(2)} \left(\gamma_{50,i} - \gamma_{50} + \gamma_{50} - D_{\rm h} \frac{\gamma_{50}}{D_{50}}\right)\right\}\right] \tag{40}$$

$$= \exp\left[\ln\left(\frac{1}{2}\right) \exp\left\{\frac{2\gamma_{50}}{\ln(2)} \left(1 - \frac{D_{\rm h}}{D_{50}}\right)\right\}\right]^{\exp\left\{\frac{2}{\ln(2)}(\gamma_{50,i} - \gamma_{50})\right\}} \tag{41}$$

$$= tcp^{\exp\left\{\frac{2}{\ln(2)}(\gamma_{50,i} - \gamma_{50})\right\}} . \tag{42}$$

Comparison of the two exponents,

$$f_i = \exp\left\{\frac{2}{\ln(2)}(\gamma_{50,i} - \gamma_{50})\right\} , \tag{43}$$

and solving for $\gamma_{50,i}$ results in

$$\begin{aligned}\gamma_{50,i} &= \gamma_{50} + \frac{\ln(2)}{2}\ln(f_i) && (44)\\ &= \gamma_{50}\left(1 + \frac{\ln(2)}{2\gamma_{50}}\ln(f_i)\right) && (45)\\ &= \gamma_{50}\, P_i\,, && (46)\end{aligned}$$

with P_i defined as

$$P_i = 1 + \frac{\ln(2)}{2\gamma_{50}}\ln(f_i)\,. \quad (47)$$

By applying Eq. (38), $D_{50,i}$ follows accordingly as

$$\begin{aligned}D_{50,i} &= \frac{\gamma_{50}}{A}\, P_i && (48)\\ &= D_{50}\, P_i\,. && (49)\end{aligned}$$

Appendix B. Derivation of model parameters: logistic model

We suppose for the logistic model,

$$\mathrm{TCP}(D) = \frac{1}{1+\exp\left\{4\gamma_{50}\left(1-\frac{D}{D_{50}}\right)\right\}}\,, \quad (50)$$

that the model parameters D_{50} and γ_{50} for the total tumor are known. The proportion of failures f_i in each of the N tumor sub-volumes were obtained at the homogeneous dose D_h at which the total TCP is given by the short notation

$$tcp = \mathrm{TCP}(D_\mathrm{h})\,. \quad (51)$$

We try to obtain the model parameters $\gamma_{50,i}$ and $D_{50,i}$ to fully describe the TCP_i for each of the N sub-volumes,

$$\mathrm{TCP}_i(D) = \frac{1}{1+\exp\left\{4\gamma_{50,i}\left(1-\frac{D}{D_{50,i}}\right)\right\}}\,, \quad (52)$$

such that the assumptions specified in Eqs. (3)-(6) are fulfilled. To evaluate the condition in Eq. (4) we need the derivative of the TCP with respect to dose for a homogeneous dose distribution,

$$\begin{aligned}\frac{\mathrm{d}}{\mathrm{d}D}\mathrm{TCP}(D) &= -\mathrm{TCP}(D)^2\ \underbrace{\exp\left\{4\gamma_{50}\left(1-\frac{D}{D_{50}}\right)\right\}}_{=\frac{1-TCP(D)}{TCP(D)}}\left(-\frac{4\gamma_{50}}{D_{50}}\right) && (53)\\ &= \mathrm{TCP}(D)\,(1-TCP(D))\,\frac{4\gamma_{50}}{D_{50}}\,, && (54)\end{aligned}$$

and we find the slopes at $D = D_{\mathrm{h}}$ for the total tumor and sub-volume i, respectively,

$$\left.\frac{\mathrm{d}}{\mathrm{d}D}\mathrm{TCP}(D)\right|_{D_{\mathrm{h}}} = tcp\,(1-tcp)\,4\,\frac{\gamma_{50}}{D_{50}} \tag{55}$$

$$\left.\frac{\mathrm{d}}{\mathrm{d}D}\mathrm{TCP}_i(D)\right|_{D_{\mathrm{h}}} = tcp^{f_i}\,(1-tcp^{f_i})\,4\,B\,, \tag{56}$$

where, according to the assumption in Eq. (6), $B = \frac{\gamma_{50,i}}{D_{50,i}}$ is a constant independent of i. To simplify the right hand side of the condition in Eq. (4) we use the product rule,

$$\left.\frac{\mathrm{d}}{\mathrm{d}D}\mathrm{TCP}(D)\right|_{D_{\mathrm{h}}} = \sum_{i=1}^{N}\underbrace{\prod_{j=1}^{N}}_{i\neq j}\mathrm{TCP}_j(D_{\mathrm{h}})\;\left.\frac{\mathrm{d}}{\mathrm{d}D}\mathrm{TCP}_i(D)\right|_{D_{\mathrm{h}}} \tag{57}$$

$$= \sum_{i=1}^{N}\underbrace{\prod_{j=1}^{N}}_{i\neq j}tcp^{f_j}\,tcp^{f_i}\,(1-tcp^{f_i})\,4B \tag{58}$$

$$= 4B\sum_{i=1}^{N}\underbrace{tcp^{1-f_i}\,tcp^{f_i}}_{=tcp}\,(1-tcp^{f_i}) \tag{59}$$

$$= 4B\,tcp\left(N-\sum_{i=1}^{N}tcp^{f_i}\right). \tag{60}$$

Setting Eq. (60) equal to the expression in Eq. (55),

$$4B\,tcp\left(N-\sum_{i=1}^{N}tcp^{f_i}\right) = 4\frac{\gamma_{50}}{D_{50}}\,tcp\,(1-tcp)\,, \tag{61}$$

and solving for B results in

$$B = \frac{\gamma_{50,i}}{D_{50,i}} = \frac{\gamma_{50}}{D_{50}}\,\frac{1-tcp}{N-\sum_{j=1}^{N}tcp^{f_j}}\,. \tag{62}$$

To determine $\gamma_{50,i}$ and $D_{50,i}$ we use the definition of TCP_i in Eq. (52) at the dose D_{h} and plug in the two assumptions, as given in Eqs. (5) and (6),

$$tcp^{f_i} = \left[1+\exp\left\{4\gamma_{50,i}\left(1-B\,\frac{D_{\mathrm{h}}}{\gamma_{50,i}}\right)\right\}\right]^{-1} \tag{63}$$

$$= \left[1+\exp\left\{4\left(\gamma_{50,i}-B\,D_{\mathrm{h}}\right)\right\}\right]^{-1}\,. \tag{64}$$

This expression can be solved for $\gamma_{50,i}$,

$$\begin{aligned} \gamma_{50,i} &= B\, D_{\mathrm{h}} + \frac{1}{4}\,\ln(tcp^{-f_i} - 1) && (65)\\ &= B\left(D_{\mathrm{h}} + \frac{1}{4B}\,\ln(tcp^{-f_i} - 1)\right) && (66)\\ &= B\,(D_{\mathrm{h}} + L_i)\,, && (67) \end{aligned}$$

with L_i defined as

$$L_i = \frac{1}{4B}\,\ln(tcp^{-f_i} - 1)\,. \quad (68)$$

By applying Eq. (62) $D_{50,i}$ follows directly,

$$\begin{aligned} D_{50,i} &= \frac{\gamma_{50,i}}{B} && (69)\\ &= D_{\mathrm{h}} + L_i\,. && (70) \end{aligned}$$